Performance improvement of transparent germanium–gallium–sulfur glass ceramic by gold doping for third-order optical nonlinearities

Feifei Chen,[1] Shixun Dai,[1,*] Changgui Lin,[1] Qiushuang Yu,[1] and Qinyuan Zhang[2]

[1] *Laboratory of Infrared Materials and Devices, The Advanced Technology Research Institute, Ningbo University, Ningbo 315211, China*

[2] *State Key Laboratory of Luminescent Materials and Devices, South China University of Technology, Guangzhou 510641, China*

[*] *daishixun@nbu.edu.cn*

Abstract: Transparent chalcogenide glass ceramics were prepared by thermally treating gold-doped germanium–gallium–sulfur glass. The gold, as nucleating agents, modified the crystallization process of the glass, resulting in the formation of nanocrystals belonging to a single α-Ga_2S_3 phase. The crystalline grains increased in number with the treatment duration while their size remained constant, leading to a high infrared transmittance of the glass ceramics. Z-scan measurements revealed the performance improvement of the α-Ga_2S_3 nanocrystals to third-order optical nonlinearities.

OCIS codes: (160.2750) Glass and other amorphous materials; (160.4236) Nanomaterial; (190.4400) Nonlinear optics, materials; (300.6420) Spectroscopy, nonlinear.

References and links

1. G. Agrawal, *Applications of Nonlinear Fiber Optics* (Academic Press, 2008).
2. P. Prabhakaran, W. J. Kim, K.-S. Lee, and P. N. Prasad, "Quantum dots (QDs) for photonic applications," Opt. Mater. Express **2**(5), 578–593 (2012), http://www.opticsinfobase.org/ome/abstract.cfm?uri=ome-2-5-578.
3. S. P. Singh and B. Karmakar, "Single-step synthesis and surface plasmons of bismuth-coated spherical to hexagonal silver nanoparticles in dichroic Ag: bismuth glass nanocomposites," Plasmonics **6**(3), 457–467 (2011).
4. T. Remyamol, H. John, and P. Gopinath, "Synthesis and nonlinear optical properties of reduced graphene oxide covalently functionalized with polyaniline," Carbon **59**, 308–314 (2013).
5. L. A. Gómez, F. E. P. Santos, A. S. L. Gomes, C. B. Araújo, L. R. P. Kassab, and W. G. Hora, "Near-infrared third-order nonlinearity of PbO-GeO_2 films containing Cu and Cu_2O nanoparticles," Appl. Phys. Lett. **92**(14), 141916 (2008).
6. W. Xiang, H. Zhao, J. Zhong, H. Luo, X. Zhao, Z. Chen, X. Liang, and X. Yang, "Synthesis and third-order optical nonlinearities of In_2S_3 quantum dots glass," J. Alloy. Comp. **553**, 135–141 (2013).
7. L. Zhang, Z. Shi, L. Zhang, Y. Zhou, and S. U. Hassan, "Fabrication and optical nonlinearities of ultrathin composite films incorporating a Keplerate type polyoxometalate," Mater. Lett. **86**, 62–64 (2012).
8. T. Hayakawa, M. Koduka, M. Nogami, J. R. Duclère, A. P. Mirgorodsky, and P. Thomas, "Metal oxide doping effects on Raman spectra and third-order nonlinear susceptibilities of thallium-tellurite glasses," Scr. Mater. **62**(10), 806–809 (2010).
9. B. J. Eggleton, B. Luther-Davies, and K. Richardson, "Chalcogenide photonics," Nat. Photonics **5**, 141–148 (2011).
10. Z. Pan, A. Ueda, R. Aga, Jr., A. Burger, R. Mu, and S. H. Morgan, "Spectroscopic studies of Er^{3+} doped Ge-Ga-S glass containing silver nanoparticles," J. Non-Cryst. Solids **356**(23-24), 1097–1101 (2010).
11. V. K. Rai, C. B. Araujo, Y. Ledemi, B. Bureau, M. Poulain, X. H. Zhang, and Y. Messaddeq, "Frequency upconversion in a Pr^{3+} doped chalcogenide glass containing silver nanoparticles," J. Appl. Phys. **103**(10), 103526 (2008).
12. M. Guignard, V. Nazabal, F. Smektala, J. L. Adam, O. Bohnke, C. Duverger, A. Moréac, H. Zeghlache, A. Kudlinski, G. Martinelli, and Y. Quiquempois, "Chalcogenide glasses based on germanium disulfide for second harmonic generation," Adv. Funct. Mater. **17**(16), 3284–3294 (2007).
13. X. F. Wang, Z. W. Wang, J. G. Yu, C. L. Liu, X. J. Zhao, and Q. H. Gong, "Large and ultrafast third-order optical nonlinearity of GeS_2-Ga_2S_3-CdS chalcogenide glass," Chem. Phys. Lett. **399**(1-3), 230–233 (2004).

#194861 - $15.00 USD Received 5 Aug 2013; revised 20 Sep 2013; accepted 3 Oct 2013; published 10 Oct 2013

14. C. Lin, L. Calvez, H. Tao, M. Allix, A. Moréac, X. Zhang, and X. Zhao, "Evidence of network demixing in GeS_2–Ga_2S_3 chalcogenide glasses: A phase transformation study," J. Solid State Chem. **184**(3), 584–588 (2011).
15. C. Lin, S. Dai, C. Liu, B. Song, Y. Xu, F. Chen, and J. Heo, "Mechanism of the enhancement of mid-infrared emission from GeS_2-Ga_2S_3 chalcogenide glass-ceramics doped with Tm^{3+}," Appl. Phys. Lett. **100**(23), 231910 (2012).
16. Y. Ledemi, B. Bureau, L. Calvez, M. Le Floch, M. Rozé, C. Lin, X. H. Zhang, M. Allix, G. Matzen, and Y. Messaddeq, "Structural investigations of glass ceramics in the Ga_2S_3-GeS_2-CsCl System," J. Phys. Chem. B **113**(44), 14574–14580 (2009).
17. G. Delaizir, P. Lucas, X. Zhang, H. Ma, B. Bureau, and J. Lucas, "Infrared glass–ceramics with fine porous surfaces for optical sensor applications," J. Am. Ceram. Soc. **90**(7), 2073–2077 (2007).
18. C. Lin, L. Calvez, M. Rozé, H. Tao, X. Zhang, and X. Zhao, "Crystallization behavior of $80GeS_220Ga_2S_3$ chalcogenide glass," Appl. Phys. A: Mater. **97**(3), 713–720 (2009).
19. C. Lin, L. Calvez, B. Bureau, H. Tao, M. Allix, Z. Hao, V. Seznec, X. Zhang, and X. Zhao, "Second-order optical nonlinearity and ionic conductivity of nanocrystalline GeS_2-Ga_2S_3-LiI glass-ceramics with improved thermo-mechanical properties," Phys. Chem. Chem. Phys. **12**(15), 3780–3787 (2010).
20. J. Ren, B. Li, G. Yang, W. Xu, Z. Zhang, M. Secu, V. Bercu, H. Zeng, and G. Chen, "Broadband near-infrared emission of chromium-doped sulfide glass-ceramics containing Ga_2S_3 nanocrystals," Opt. Lett. **37**(24), 5043–5045 (2012).
21. A. Edgar, G. V. M. Williams, and J. Hamelin, "Optical scattering in glass ceramics," Curr. Appl. Phys. **6**(3), 355–358 (2006).
22. H. Guo, H. Tao, Y. Zhai, S. Mao, and X. Zhao, "Raman spectroscopic analysis of GeS_2-Ga_2S_3-PbI_2 chalcohalide glasses," Spectrochim. Acta A Mol. Biomol. Spectrosc. **67**(5), 1351–1356 (2007).
23. M. Klopfer and R. K. Jain, "Plasmonic quantum dots for nonlinear optical applications [Invited]," Opt. Mater. Express **1**(7), 1353–1366 (2011), http://www.opticsinfobase.org/ome/abstract.cfm?uri=ome-1-7-1353.
24. E. W. Van Stryland, M. A. Woodall, H. Vanherzeele, and M. J. Soileau, "Energy band-gap dependence of two-photon absorption," Opt. Lett. **10**(10), 490–492 (1985).
25. C. Lin, L. Calvez, L. Ying, F. Chen, B. Song, X. Shen, S. Dai, and X. Zhang, "External influence on third-order optical nonlinearity of transparent chalcogenide glass-ceramics," Appl. Phys. A: Mater. **104**(2), 615–620 (2011).
26. H. Guo, C. Hou, F. Gao, A. Lin, P. Wang, Z. Zhou, M. Lu, W. Wei, and B. Peng, "Third-order nonlinear optical properties of GeS_2-Sb_2S_3-CdS chalcogenide glasses," Opt. Express **18**(22), 23275–23284 (2010), http://www.opticsinfobase.org/oe/abstract.cfm?uri=oe-18-22-23275.
27. D. Marchese, M. De Sario, A. Jha, A. K. Kar, and E. C. Smith, "Highly nonlinear GeS_2-based chalcohalide glass for all-optical twin-core-fiber switching," J. Opt. Soc. Am. B **15**(9), 2361–2370 (1998).
28. G. Lenz, J. Zimmermann, T. Katsufuji, M. E. Lines, H. Y. Hwang, S. Spälter, R. E. Slusher, S. W. Cheong, J. S. Sanghera, and I. D. Aggarwal, "Large Kerr effect in bulk Se-based chalcogenide glasses," Opt. Lett. **25**(4), 254–256 (2000).
29. K. Tanaka, "Two-photon optical absorption in amorphous materials," J. Non-Cryst. Solids **338–340**, 534–538 (2004).
30. M. Sheik-Bahae, D. J. Hagan, and E. W. Van Stryland, "Dispersion and band-gap scaling of the electronic Kerr effect in solids associated with two-photon absorption," Phys. Rev. Lett. **65**(1), 96–99 (1990).

1. Introduction

The past decade has witnessed significant progress in the development of nonlinear photonic devices [1]; however, ultrafast information transmission and exploitation of new materials [2–4] with large optical nonlinearity remain a challenge. Three parameters, namely, nonlinear refractive index (γ), nonlinear absorption coefficient (β), and nonlinear response time (τ), need to be considered in the evaluation of the performance of third-order nonlinear (TON) materials in different applications. For examples, performance of nonlinear waveguides relies on γ of the materials as well as their effective core area (A_{eff}); optical solution generation requires TON materials with positive or negative γ; all-optical switching (AOS) requires TON materials with high γ but low β and τ, and optical limiting (OL) requires only materials with high β. Therefore, much effort [5–8] has been exerted to design materials that match the specifications of each particular TON-based optical device, particularly glass materials whose properties can be readily modified by varying compositions, preparation processes, and post-treatments.

Chalcogenide glass as an excellent infrared (IR) window material is well-known to exhibit high TON performance [9]. Among the various types of chalcogenide glass, those based on germanium–gallium–sulfur (Ge–Ga–S or GGS) glass system [10–13] have been extensively studied for their good visible transparency, high rare earth solubility, and desirable chemical and thermal stabilities. Recent studies [14–17] have analyzed the crystallization behavior of

#194861 - $15.00 USD Received 5 Aug 2013; revised 20 Sep 2013; accepted 3 Oct 2013; published 10 Oct 2013

GGS glass and reported the preparation of GGS glass ceramics (GGS-GCs) that possess better optical and mechanical properties as well as unchanged high IR transparency. The crystal species in GGS-GCs rely on glass composition as well as the processing method. The formation of GGS-based glass ceramics from the combination of Ga_2S_3 crystals with GeS_2 (pure GGS) [18], Li_4GeS_4 (containing LiI) [19], GaS, or CsCl (containing CsCl) [16] crystals has been reported; the optical properties of these ceramics vary significantly with the presence of different crystal phases. Minimal effort [20] has also been exerted to prepare and characterize GGS-GCs with a single crystal phase; such is important in understanding the optimal crystallization for particular optical behaviors.

In this study, transparent GGS-GCs containing a single α-Ga_2S_3 crystal phase were prepared by incorporating a small amount of gold into GGS glass. The TON performance of GGS glass was improved because of the formation of α-Ga_2S_3 crystals. The application potential of this type of glass in TON-based devices was evaluated based on the figure of merit.

2. Experimental

GGS glass with the molar composition of $Ga_{10}Ge_{25}S_{65}$ and the same type of glass doped with 0.5 wt% gold (referred to as GGS-Au-0) was prepared from high-purity polycrystalline germanium (5 N), gallium (5 N), sulfur (5 N), and gold powder (4 N). Raw materials were carefully weighed (10 g) and sealed in evacuated (10^{-4} Pa) silica glass ampoules. The materials were then melted at 950 °C in a rocking furnace for 24 h and then quenched in water. The glass transition temperatures (T_g) of the quenched glasses were measured with a differential scanning calorimetry (DCS) device (TA-Q series). The obtained T_g of GGS-Au-0 was 445 °C, 3 °C lower than that of the host glass. This temperature value indicates the negative effect of gold on the network compactness of GGS glass. The two glass rods were then annealed (10 °C below T_g), cut into discs (ϕ 10 mm × 0.5 mm), and optically polished. Subsequently, GGS-Au-0 was crystallized by heating at 2 °C/min to a designated temperature (10 °C above T_g) and maintained for 9, 18, 36, and 72 h (labeled as GGS-Au-9, 18, 36, and 72). The GGS glass was also treated at 10 °C above its T_g for 64 h for comparison.

To analyze the crystalline nature of the samples, powder X-ray diffraction (XRD) patterns were recorded with a Bruker AXS D2 PHASER diffractometer (voltage = 30 kV; current = 10 mA; Cu Ka radiation) with a step width of 0.02°. Vickers-hardness (*HV*) of the samples was measured by a Everone MH-3 microhardness meter with a charge of 100 g for 5 s. Optical absorption spectra were obtained with a Perkin-Elmer Lambda 950UV/VIS/NIR spectrophotometer at a range of 400 nm to 2000 nm. Fourier transform infrared (FTIR) transmission measurements were performed at the infrared range of 2.5 μm to 13 μm with a Thermo Scientific Nicolet 380 FT-IR spectrometer. Scanning electron microscopic (SEM) measurements were performed with a Tescan VEGA3 SB-Easyprobe scanning electron microscope on a fresh crack created on the sample surface (coated with gold in a nitrogen atmosphere). Raman spectra were obtained through back scattering (180°) configuration with a Renishaw inVia laser confocal Raman spectrometer with an excitation wavelength of 488 nm and a frequency resolution of ± 1 cm^{-1}. The laser intensity was set between 0.1 mW to 0.5 mW, and the exposure time was 10 s.

The TON properties of the samples at the wavelength of 800 nm were characterized by single beam Z-scan technique. A Coherent Mira 900-D Ti:sapphire laser with a pulse duration of 200 fs was used as a laser source. Laser pulses were operated at 76 MHz with a beam waist (ω_0) of 24 μm detected by CCD. The incident laser power was set to 60 mW corresponding to irradiance of 1.42 GW/cm^2 at focus. The measurements were repeated five times at different areas on the sample surface to minimize the experimental error. All of the above optical measurements were conducted at room temperature.

#194861 - $15.00 USD Received 5 Aug 2013; revised 20 Sep 2013; accepted 3 Oct 2013; published 10 Oct 2013

3. Results and discussion

X-ray diffraction studies were conducted on the glass and heat-treated samples to confirm their amorphous and crystalline nature, respectively. Figure 1(a) shows the XRD patterns of the GGS glass and its heat-treated samples. The broad hump without any distinct peak confirms the amorphous nature of the glass matrix. After 64 h of heat treatment at 10 °C above its T_g, the glass on both surfaces and on the inner side were highly crystallized as illustrated in the XRD patterns. The diffraction peaks of the treated GGS glass are sharp and abundant, indicating a large grain number and size. The possible assignments of these peaks may be GeS_2 (JCPDS-file No.: 29–644, 30–597) and Ga_2S_3 (JCPDS-file No.: 43–619). According to a previous study [18] on GGS-based glass ceramics, the precipitation of the Ga_2S_3 phase is prioritized over that of the GeS_2 phase; long heat treatment duration causes the presence of both crystal phases in the chalcogenide glass matrix. The results of this previous study are consistent with the results of the present study.

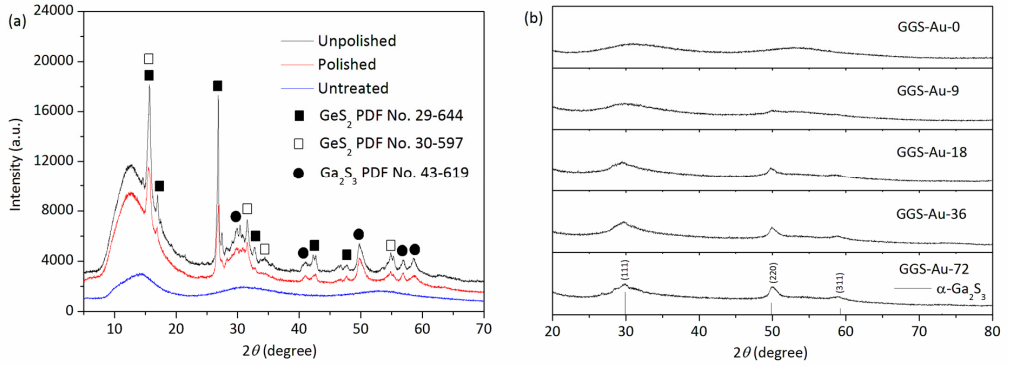

Fig. 1. (a) XRD patterns of the GGS glass and the glasses heat treated for 64 hours (including surface polished and unpolished); (b) XRD patterns of the GGS-Au series.

GGS-Au-0 is amorphous as shown in Fig. 1(b). After heat treatment, diffraction peaks attributed to α-Ga_2S_3 (JCPDS-file No.: 65–7839) appeared and grew with treatment duration. In contrast to the treated GGS glasses, the diffraction intensities of the GGS-Au series are much weaker and broader in spite of the longer treatment duration of GGS-Au-72, indicating the presence of much finer α-Ga_2S_3 crystals in the gold-doped glass matrix. The diffraction peaks of GGS-Au-72 show no significant enhancement compared with those of GGS-Au-36, indicating that the crystallization of the α-Ga_2S_3 phase saturated after 36 h of treatment. The introduction of gold to the GGS glass suppressed the formation of Ge-related phases but facilitated the formation of the α-Ga_2S_3 crystal phase. The gold ions with the largest size in the GGS matrix functioned as nucleating agents only for the α-Ga_2S_3 crystals during the thermal process. Further, as listed in Table 1, Vickers-hardness (*HV*) of the glass ceramics shows the maximum value in GGS-Au-9, while extension of thermal treatment caused a decrease of hardness. However, all *HV* of the GGS-Au series is higher than that of the pure GGS glass (*HV* = 239 Kg·mm^2), indicating better mechanical properties from doping of gold and subsequent thermal treatment.

Figure 2 presents the absorption spectra of the GGS-Au series. The UV cut-off at approximately 500 nm is consistent with the yellow color of the samples as seen in the inset. The visible transparency of the samples decreased slightly with the increase in the treatment duration. The red-shifting of the UV cut-off caused by the increasing number of α-Ga_2S_3 crystals is responsible for this behavior, which is a result of Rayleigh-Gans type scattering [21] that depends on the size and number of crystals. Sample GGS-Au-36 has a similar UV cut-off to that of GGS-Au-72, indicating that the formation of α-Ga_2S_3 crystals reached the maximum level after 36 h of treatment. This finding is in agreement with the XRD

#194861 - $15.00 USD Received 5 Aug 2013; revised 20 Sep 2013; accepted 3 Oct 2013; published 10 Oct 2013

observations. Furthermore, the effect of scattering from the α-Ga_2S_3 crystals to the optical transmittance significantly weakened at wavelengths greater than 1000 nm. As shown in the FTIR spectra in the inset of Fig. 2, the IR transparencies of the GGS-Au series varied slightly, all of which maintained constant IR cut-off at 12 μm. By contrast, the obtained spectrum of the treated GGS glass exhibited poor IR transparence because of high scattering losses from large crystals.

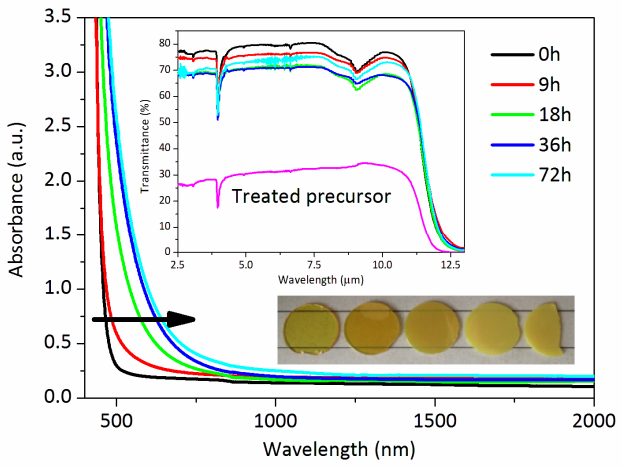

Fig. 2. Vis-NIR absorption spectra of the GGS-Au series. Insets are their photograph and FTIR spectra.

The formation of α-Ga_2S_3 crystals was further confirmed by SEM as presented in Fig. 3. The amorphous GGS glass in Fig. 3(a) has a clean and homogenous surface, indicating the absence of a phase with different electric conductivities. The treated GGS glass in Fig. 3(b) contains numerous density crystals with various shapes and sizes (from 100 nm to over 1000 nm), consistent with the sharp and abundant diffraction peaks in its XRD pattern. The GGS-Au series is shown in Figs. 3(c) to 3(f). The sample subjected to 9 h of treatment exhibits a fine distribution of α-Ga_2S_3 crystals. The crystals have a watermark configuration and are below 50 nm in size; thus, they can be considered nanocrystals (NCs). As the treatment duration increased, the density of the NCs increased significantly. However, their sizes remained unchanged compared with those in GGS-Au-9. No grain agglomeration occurred, which is a reasonable explanation for the constant IR transmittance of the GGS-Au glass ceramics.

#194861 - $15.00 USD Received 5 Aug 2013; revised 20 Sep 2013; accepted 3 Oct 2013; published 10 Oct 2013

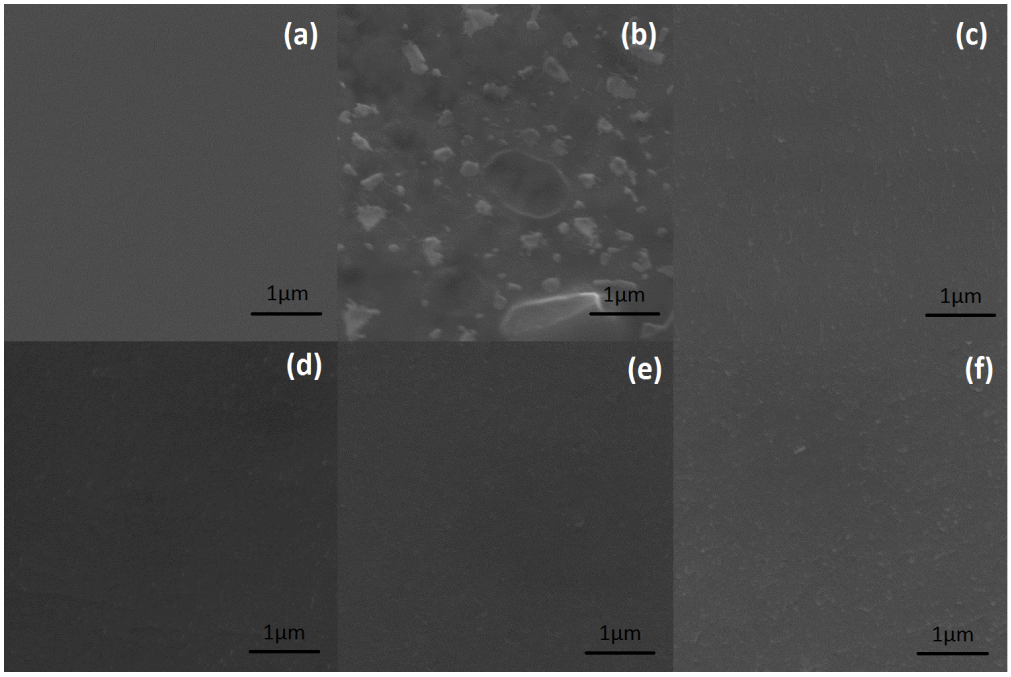

Fig. 3. SEM images of the glass and glass ceramic samples: (a) the GGS glass; (b) the treated GGS glass; (c) GGS-Au-9; (d) GGS-Au-18; (e) GGS-Au-36; (f) GGS-Au-72.

Raman spectral studies were conducted to understand the evolution of the GGS-Au glass network through heat treatment. The most evident evolution of the Raman signal with thermal treatment was located from 230 cm^{-1} to 290 cm^{-1} as can be seen in Fig. 4. Two peaks appeared at 240 and 255 cm^{-1} respectively, and they grew with treatment duration. The peak at 270 cm^{-1} exhibited the opposite and disappeared after 36 h of treatment. Previous studies [14, 16] on GGS-based glass ceramics have demonstrated that a Raman signal in the abovementioned range is a characteristic vibration of metal–metal bonds and that heavy metal bonds vibrate at low frequencies. The peak at approximately 270 cm^{-1} is a typical vibration mode of Ga–Ga homopolar bonds in [$S_3Ga–GaS_3$] ethane-like units, and the disappearance of Raman signal at this frequency range is an indication of the breakage of such homopolar bonds under heat treatment. The newly formed peak at 255 cm^{-1} can be assigned to Ge–Ge homopolar bonds in [$GeS_{4-x}–Ge_x$] entities. They appeared and situated in the amorphous glass matrix after the gallium was separated from the host glass network after continuous heat treatment, which partly compensated the loss of Ga–Ga bonds. For the peak appeared at 240 cm^{-1} in the GGS-Au GCs, its location is consistent with that of main Raman peak in crystalline Ga_2S_3 [22], namely the vibration mode of S–Ga–S links within in the edge-shared GaS_4 tetrahedra, thus it is reasonable to assign this band to vibration of the above mentioned bond structure, which is also in agreement with the variation tendency of number density of Ga_2S_3 nanocrystals in the glass ceramic samples.

#194861 - $15.00 USD Received 5 Aug 2013; revised 20 Sep 2013; accepted 3 Oct 2013; published 10 Oct 2013

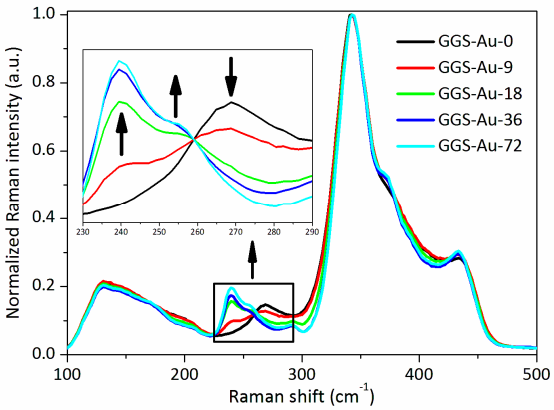

Fig. 4. Raman spectra of the GGS-GCs. The inset is the enlarged spectra at a Raman shift range of 230 cm^{-1} to 290 cm^{-1}.

According to above spectral and morphology studies, schematic of the localized GGS-Au glass matrix that involved in the crystallization process was proposed and shown in Fig. 5. It should be noted that no S–S bond was formed due to sulfur shortage in the chemical composition ($Ga_{10}Ge_{25}S_{65}$ in mol%) of the GGS glass. Further, as indicated in the Raman spectra, Ga–Ga homopolar bonds is the dominate component of metal bonds in present GGS glass matrix, and they were broken during heat treatment and completely disappeared after 36 h treatment. It favored the formation of another metal bond, namely Ge–Ge homopolar bonds in the glass matrix. They only existed in glass phase of the GCs, which partly compensated the loss of Ga–Ga bonds. The role of gold, as demonstrated above performed like nucleating agent which varied significantly the crystallization process of GGS glass, and they were surrounded by the regular S–Ga bonding structures, namely the α-Ga_2S_3 crystals as a result of heat treatment.

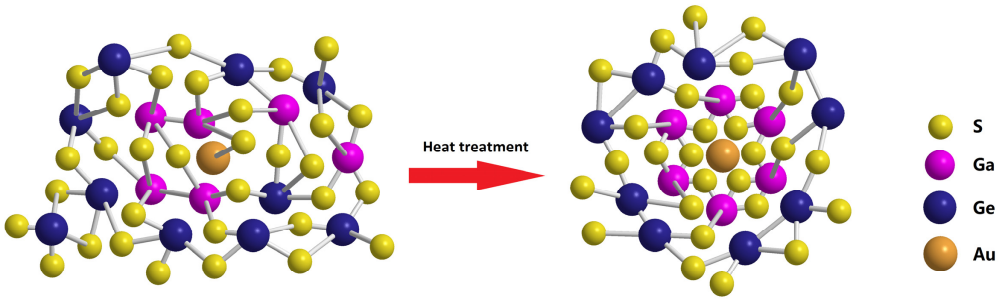

Fig. 5. Schematic of the localized GGS-Au glass matrix that involved in crystallization process.

The above experimental observations indicate that the gold ions facilitated the formation of α-Ga_2S_3 NCs, which grew in density as the treatment duration increased. Crystallization ceased after 36 h of heat treatment without agglomeration, indicating that all the nucleating agents (Au) were covered by the α-Ga_2S_3 crystals. Studying the dependency of the TON properties of GGS-GCs on the number density of α-Ga_2S_3 NCs is therefore critical in understanding the electromagnetic interactions among chalcogenide nanocrystals under high laser irradiance. Figures 6(a) and 6(b) show the closed-aperture (CA) and open-aperture (OA) Z scans of the GGS-Au series, respectively. As seen in the former, the peak with a valley configuration manifests the self-defocusing behavior of the samples, namely, the positive value of nonlinear refraction (γ). The gap between the normalized transmittance valley and the

#194861 - $15.00 USD Received 5 Aug 2013; revised 20 Sep 2013; accepted 3 Oct 2013; published 10 Oct 2013

peak is largest in the curve of GGS-Au-9. The gap decreased with the extension of treatment duration, illustrating the evolution tendency of the γ value of GGS-GCs. The calculated results shown in Table 1 indicate that the maximum γ value obtained from GGS-Au-9 reached 2.4×10^{-17} m^2/W, which is twice that of GGS-Au-0. As crystallization reached the maximum level (36 h of heat treatment), the minimum γ value of the GGS-GCs was obtained; however, the value is still higher than that of GGS-Au-0. The enhanced nonlinear refraction behavior of the GGS-Au series is evidence of the local field effect (LFE) caused by the α-Ga_2S_3 NCs. Small NCs or quantum dots cause strong LFE because of their strong size confinement [23]. In the experimental results, the TON response was caused by weak size confinement (NC radius over 10 nm) and was related to the density of NCs (distance between them). The electronic process changed significantly because of the formation of condensed crystal fields, namely, LFE between the adjacent α-Ga_2S_3 NCs, under high laser irradiance, resulting in increments in nonlinear refraction. The average intensity of the polar fields weakened because of the offsetting behavior of charge interactions between NCs as their density increased, leading to the reduction in the γ value of the NC-embedded GCs.

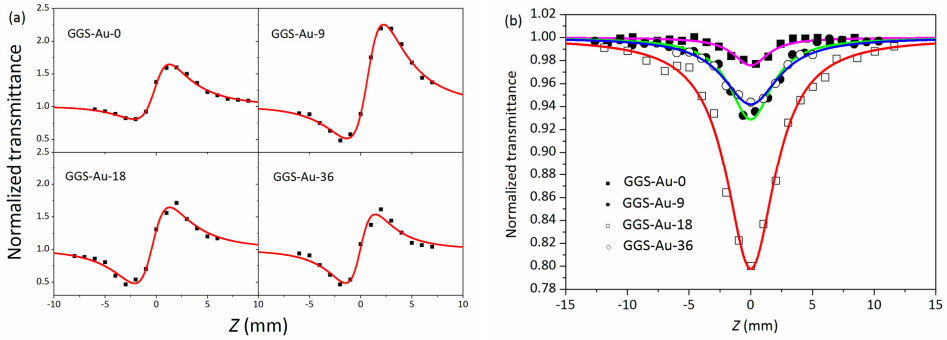

Fig. 6. Z-scan curves of the GGS-Au series: (a) closed aperture Z-scans; (b) open aperture Z-scans.

The single valley in the center of the OA Z scans is an indication of two-photon absorption (TPA), and the depth of the valley indicates the magnitude of the TPA coefficient (β). The β values were obtained by fitting the curves with a theoretical TPA process model [24]. The values are summarized in Table 1. The largest β value was obtained from GGS-Au-18; its value of 3.44×10^{-11} m/W is over 10 times that of GGS-Au-0. The β value of GGS-Au-9 is significantly lower than that of GGS-Au-18, indicating that LEF enhancement in TPA reached the maximum level at high NC density. Similar experimental results were obtained from the β-GeS_2-embedded GGS-GCs [25]. All the β values of the GGS-GCs are larger than those of GGS-Au-0 and are comparable to those of chalcogenide glass with high TON performance found in literature [26, 27]. This finding reveals the potential application of GGS-GCs in related optical limiting devices.

Table 1. Vickers-hardness (*HV*), optical band gap (E_{opg}) and TON parameters of the GGS-Au series and some chalcogenide glasses in literature

Sample no.	*HV* (Kg·mm^2) ± 2	E_{opg} (eV) ± 0.01	γ (10^{-17} m^2/W) ± 0.1	β (10^{-12} m/W) ± 0.1	*F* ± 0.1
GGS-Au-0	252	2.84	1.2	2.9	0.2
GGS-Au-9	273	2.83	2.4	9.5	0.3
GGS-Au-18	247	2.75	1.8	34.4	1.5
GGS-Au-36	241	2.63	1.6	13.6	0.7
60GeS_2-40Sb_2S_3 [26]	-	1.95	0.67	17.1	4.1
75GeS_2-10Ga_2S_3-10CsI-0.5Ag_2S [27]	-	-	0.75	22.0	2.1
As_2Se_3 [28]	-	1.77	1.2	24.5	0.5

#194861 - $15.00 USD Received 5 Aug 2013; revised 20 Sep 2013; accepted 3 Oct 2013; published 10 Oct 2013

For AOS devices wherein nonlinear glass materials can be applied, the corresponding figure of merit (defined as $F = \lambda\beta/\gamma$) is utilized to evaluate the suitability of synthesized materials, thereby compromising TPA loss and nonlinear refractive index. The value of F must be less than 1 for the material to be deemed suitable. For the GGS-Au series, the calculated results show that the enhanced TPA of the GCs reduced their AOS performance and that GGS-Au-18 did not meet the abovementioned criterion ($F < 1$). However, when the photon energy ($h\nu$) is defined with the absorption coefficient of 1000 cm^{-1} as the optical band gap (E_{opg}) [28], the normalized photon energy values ($h\nu/E_{opg}$) of the GGS-Au series are 0.54 and 0.59, indicating the presence of TPA resonance [29]. This type of resonance is a characteristic of amorphous materials (e.g., glass) that exhibit direct bandgap behaviors [30]. Therefore, resonant TPA would be weakened or eliminated at long wavelengths, especially in the optical communication band in which the $h\nu/E_{opg}$ values of the GGS-Au series are less than 0.5.

4. Conclusions

The formation of nanocrystals belonging to a single α-Ga_2S_3 phase within gold-doped Ge–Ga–S chalcogenide glass was demonstrated in this study. The gold functioned as nucleating agents for the α-Ga_2S_3 nanocrystals, resulting in high IR transmittance of the glass ceramics. The improvement in the performance of the α-Ga_2S_3 nanocrystals was a function of their density values. The maximum increasing amplitude at nonlinear refraction and two-photon absorption were found at two specified crystal density values.

Acknowledgments

This work was partially supported by the National Natural Science Foundation of China (Grant No. 61308094), the International Science & Technology Cooperation Program of China (Grant No. 2011DFA12040), National Program on Key Basic Research Project (973 Program) (Grant No. 2012CB722703), Program for Innovative Research Team of Ningbo City (Grant No. 2009B21007), the Open Fund of the State Key Laboratory of Luminescent Materials and Devices (South China University of Technology), and Zhejiang Provincial Natural Science Foundation of China (Grant No. LQ12F05003). The study was also sponsored by K.C. Wong Magna Fund in Ningbo University.

#194861 - $15.00 USD Received 5 Aug 2013; revised 20 Sep 2013; accepted 3 Oct 2013; published 10 Oct 2013